ACS Combinatorial Science

Research Article

Cite This: ACS Comb. Sci. 2019, 21, 598−607

pubs.acs.org/acscombsci

High-Affinity $\alpha_5\beta_1$-Integrin-Selective Bicyclic RGD Peptides Identified via Screening of Designed Random Libraries

Dominik Bernhagen,[†] Vanessa Jungbluth,[‡] Nestor Gisbert Quilis,[‡] Jakub Dostalek,[‡] Paul B. White,[¶] Kees Jalink,[⊥] and Peter Timmerman*[,†,§]

[†]Pepscan Therapeutics, Zuidersluisweg 2, 8243 RC Lelystad, the Netherlands

[‡]Biosensor Technologies, AIT Austrian Institute of Technology GmbH, Konrad-Lorenz-Straße 24, 3430 Tulln, Austria

[¶]Institute for Molecules and Materials, Radboud University, Heyendaalseweg 135, 6525 AJ Nijmegen, the Netherlands

[⊥]The Netherlands Cancer Institute, Plesmanlaan 21, 1066 CX Amsterdam, the Netherlands

[§]Van't Hoff Institute for Molecular Sciences, University of Amsterdam, Science Park 904, 1098 XH Amsterdam, the Netherlands

Supporting Information

ABSTRACT: We report the identification of high-affinity and selectivity integrin $\alpha_5\beta_1$-binding bicyclic peptides via "designed random libraries", that is, the screening of libraries comprising the universal integrin-binding sequence Arg-Gly-Asp (RGD) in the first loop in combination with a randomized sequence (XXX) in the second loop. Screening of first-generation libraries for $\alpha_5\beta_1$-binding peptides yielded a triple-digit nanomolar bicyclic $\alpha_5\beta_1$-binder ($\mathbf{C}_{T3}$RGD$\mathbf{c}_{T3}$AYG$\mathbf{C}_{T3}$, IC_{50} = 406 nM). Next-generation libraries were designed by partially varying the structure of the strongest first-generation lead inhibitor and screened for improved affinities and selectivities for this receptor. In this way, we identified three high-affinity $\alpha_5\beta_1$-binders ($\mathbf{C}_{T3}$RGD$\mathbf{c}_{T3}$AYJ$\mathbf{C}_{T3}$, J = D-Leu, IC_{50} = 90 nM; $\mathbf{C}_{T3}$RGD$\mathbf{c}_{T3}$AYa$\mathbf{C}_{T3}$, IC_{50} = 156 nM; $\mathbf{C}_{T3}$RGD$\mathbf{c}_{T3}$AWG$\mathbf{C}_{T3}$, IC_{50} = 173 nM), of which one even showed a higher $\alpha_5\beta_1$-affinity than the 32 amino acid benchmark peptide knottin-RGD (IC_{50} = 114 nM). Affinity for $\alpha_5\beta_1$-integrin was confirmed by SPFS analysis showing a K_d of 4.1 nM for Cy5-labeled RGD-bicycle $\mathbf{C}_{T3}$RGD$\mathbf{c}_{T3}$AYJ$\mathbf{C}_{T3}$ (J = D-Leu) and a somewhat higher K_d (9.0 nM) for Cy5-labeled knottin-RGD. The $\alpha_5\beta_1$-bicycles, for example, $\mathbf{C}_{T3}$RGD$\mathbf{c}_{T3}$AYJ$\mathbf{C}_{T3}$ (J = D-Leu), showed excellent selectivities over $\alpha_v\beta_5$ (IC_{50} ratio $\alpha_5\beta_1/\alpha_v\beta_5$ between <0.009 and 0.039) and acceptable selectivities over $\alpha_v\beta_3$ (IC_{50} ratios $\alpha_5\beta_1/\alpha_v\beta_3$ between 0.090 and 0.157). In vitro staining of adipose-derived stem cells with Cy5-labeled peptides using confocal microscopy revealed strong binding of the $\alpha_5\beta_1$-selective bicycle $\mathbf{C}_{T3}$RGD$\mathbf{c}_{T3}$AWG$\mathbf{C}_{T3}$ to integrins in their natural environment, illustrating the high potential of these RGD bicycles as markers for $\alpha_5\beta_1$-integrin expression.

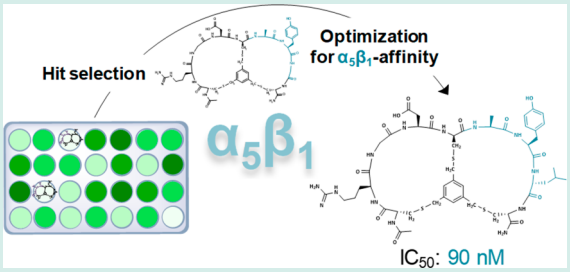

KEYWORDS: *RGD, integrin, peptide−protein interaction, ELISA, bicyclic peptide, library screening, SPFS*

INTRODUCTION

Integrins, a group of 24 different heterodimeric transmembrane proteins,[1,2] are involved in many cellular processes, such as signaling, proliferation, migration, and differentiation.[3,4] Integrin expression is a dynamic process that depends on the microenvironment and developmental age of cells.[1] For example, epidermal and neural stem cells solely overexpress the β_1-subunit, while adipose-tissue-derived stem cells overexpress the heterodimeric $\alpha_5\beta_1$ in undifferentiated state, as well as during chondrogenic differentiation.[5]

High levels of $\alpha_5\beta_1$-integrin expression increase the invasiveness of breast cancer cells into 3D collagen fiber matrices by 3-fold compared to cells with low levels of $\alpha_5\beta_1$ expression.[6] Integrins also exhibit extensive crosstalk among each other.[7] For example, integrin $\alpha_5\beta_1$ is a regulator of angiogenesis and was furthermore reported to control integrin $\alpha_v\beta_3$ expression during in vitro migration and in vivo angiogenesis.[8] Moreover, $\alpha_5\beta_1$ efficiently mediates fibronectin fibrillogenesis[9] and also binds osteopontin, fibrillin, and thrombospondin.[10] Several high-affinity $\alpha_5\beta_1$-integrin binders not displaying any selectivity toward other integrins have been reported, such as knottin-RGD ($\alpha_v\beta_3/\alpha_v\beta_5/\alpha_5\beta_1$-binder)[11−13] or echistatin (binds $\alpha_v\beta_3$, $\alpha_v\beta_5$, $\alpha_v\beta_6$, $\alpha_v\beta_8$, $\alpha_5\beta_1$, and $\alpha_{IIb}\beta_3$).[14,15] Ligands with improved $\alpha_5\beta_1$ selectivity, such as the 5-mer PHSCN (ATN-161) that proved to inhibit $\alpha_5\beta_1$ in immunoassays[15] and in vivo,[16,17] recently raised considerable interest as potential cancer therapeutics. Also, high-affinity peptidomimetic ligands with $\alpha_5\beta_1$ selectivity were reported by Heckmann et al. as potential antiangiogenic cancer therapeutics.[18] When covalently linked to a gold surface, these ligands showed a much higher level of cell adhesion to $\alpha_5\beta_1$-transfected fibroblasts as compared to $\alpha_v\beta_3$-transfected cells.[19] However, these peptidomimetics require complex multistep syntheses (in particular the building blocks), which

Received: April 18, 2019
Revised: June 5, 2019
Published: July 3, 2019

DOI: 10.1021/acscombsci.9b00081
ACS Comb. Sci. 2019, 21, 598−607

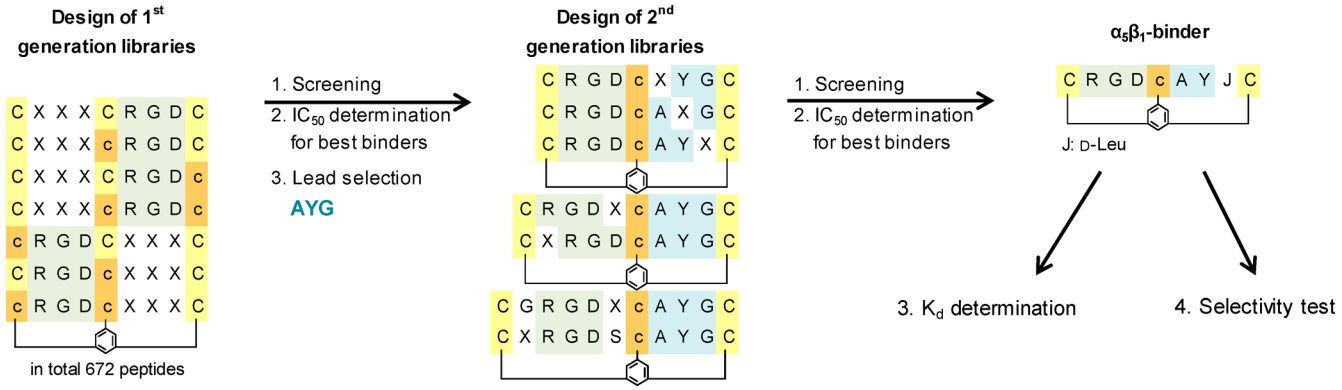

Figure 1. Methodology for the structural design, affinity selection, identification, and characterization of high affinity bicyclic peptides to integrin $\alpha_5\beta_1$.

does (not yet) allow for economically feasible bulk production. There is a strong need for novel peptidic $\alpha_5\beta_1$-integrin binders that could circumvent this problem. Very recently, Kapp et al. reported *N*-methylated, cyclic *iso*DGR peptides with high $\alpha_5\beta_1$-selectivity over integrins $\alpha_v\beta_6$ and $\alpha_v\beta_3$.[20] Our group recently described strong and selective $\alpha_v\beta_3$-binders obtained via a "designed random library" based approach involving medium-throughput screening of libraries of bicyclic peptides comprising both an RGD-loop combined with a second randomized loop.[21,22] Bicyclic CLIPS peptides[23] represent a group of target-specific and proteolytically stable compounds that recently showed great potential for therapeutic drug development.[24−26] For example, the bicyclic peptide $AC_{T3}SDRFRNC_{T3}PADEALC_{T3}G$ (**T3** = scaffold derived from 1,3,5-trisbromomesitylene) was identified as a nanomolar plasma kallikrein-inhibitor (K_i = 1.5 nM) consisting of a consensus binding motif (SDRFRN) in combination with an optimized supporting sequence (PADEAL).[27]

The excellent integrin $\alpha_v\beta_3$-affinities and selectivities observed with bicyclic RGD-peptides[21] prompted us to test the same libraries also for binding to the $\alpha_5\beta_1$ integrin receptor. Here, we describe the results of those screenings together with the structural optimization and characterization of high-affinity bicyclic RGD-binders to integrin $\alpha_5\beta_1$.

RESULTS AND DISCUSSION

Design of RGD Peptide Libraries. We designed linear peptide libraries consisting of two separate binding motifs, surrounded by three cysteines. The first motif is the well-known RGD sequence that should provide the basic integrin affinity, while the second motif contains a random-diversity sequence that is intended to provide integrin-selectivity. The motifs are surrounded by cysteines that allow for the double CLIPS-cyclization via 1,3,5-tris(bromomethyl) benzene (**T3**, see Figure S6A), and hence the formation of a bicyclic peptide comprising two different loops is achieved. According to the design of high-affinity monocyclic RGD-peptides, as reported by Dechantsreiter et al.,[28] we synthesized bicyclic peptide libraries containing two "5-mer" loops, that is, RGD and XXX, each enclosed by L- or D-cysteines. Seven libraries, each containing 96 peptides, were converted to bicyclic peptides via **T3** ($C_{T3}XXXC_{T3}RGDC_{T3}$, $C_{T3}XXXc_{T3}RGDC_{T3}$, $C_{T3}XXXC_{T3}RGDc_{T3}$, and $C_{T3}XXXc_{T3}RGDc_{T3}$, $c_{T3}RGDC_{T3}XXXC_{T3}$, $C_{T3}RGDc_{T3}XXXC_{T3}$, $c_{T3}RGDc_{T3}XXXC_{T3}$, Figure 1). All 34 amino acid building blocks that were applied in this study are listed in the Supporting Information (Table S-1). For more detailed information on the design, we kindly refer to ref 21.

General Procedure for RGD Bicycle Library Screening. We screened the bicyclic RGD-peptide libraries for integrin-binding using our recently developed and published protocol for a competition ELISA (for experimental conditions, see Table S-2).[22]

All 672 bicyclic RGD-peptides were screened for inhibition of biotinylated knottin-RGD binding to integrin $\alpha_5\beta_1$ and sorted for the highest degree of inhibition. A second screening with the best hits from the first screening was performed at 2.5 μM to further fine tune the differences in integrin affinities. Following screening of the various crude bicycle peptide libraries, the best binding bicycles were resynthesized and HPLC-purified, followed by determination of their IC_{50} values.

Screening Data for $\alpha_5\beta_1$-Binding Bicycles. We screened the first-generation bicycle libraries for high-affinity binding to integrin $\alpha_5\beta_1$. Only nine out of 672 peptides (1.3%) showed >70% inhibition, and all of these peptides comprised the RGD-sequence in the left loop, enclosed by an N-terminal L-Cys and a central D-Cys. Still 4% of the peptides (29) showed >50% inhibition, whereas 80% (540 peptides) showed inhibition levels <30%. Two bicycles, that is, $C_{T3}RGDc_{T3}AYGC_{T3}$ (100%) and $C_{T3}RGDc_{T3}NWGC_{T3}$ (91%) showed >90% inhibition of (biotinylated) knottin-RGD binding after the second screening. For $C_{T3}RGDc_{T3}AYGC_{T3}$ an IC_{50} value of 406 nM was determined, whereas bicycle $C_{T3}RGDc_{T3}NWGC_{T3}$ exhibited an IC_{50} > 2 μM (Figure 2). The IC_{50} value for $C_{T3}RGDc_{T3}AYGC_{T3}$ was much lower than observed for *cyclo*-[KRGDf], cilengitide (each >10 μM), and slightly higher than for knottin-RGD (114 nM). The unexpected discrepancy between inhibition values of $C_{T3}RGDc_{T3}NWGC_{T3}$ in the screening (91% at 10 μM) and IC_{50} (>2 μM) may be explained by the fact that "polymeric" impurities in the crude peptide sample create an "apparent" inhibition value that is much lower than the IC_{50} value as determined using the purified bicycle peptide. On the basis of the sequence of $C_{T3}RGDc_{T3}AYGC_{T3}$, we designed a set of second generation libraries, including (1) a full position-replacement analysis of the AYG-loop (i.e., $C_{T3}RGDc_{T3}XYGC_{T3}$, $C_{T3}RGDc_{T3}AXGC_{T3}$, $C_{T3}RGDc_{T3}AYXC_{T3}$), (2) the RGD-loop extended by an additional amino acid "X", while keeping the "AYG"-loop constant (i.e., $C_{T3}RGDXc_{T3}AYGC_{T3}$, $C_{T3}XRGDc_{T3}AYGC_{T3}$), and (3) the extended 5-mer loops "GRGDX" and "XRGDS" in combination with a constant "AYG"-loop (i.e.,

DOI: 10.1021/acscombsci.9b00081
ACS Comb. Sci. 2019, 21, 598−607

Peptide	IC_{50} [nM]
1st generation	
C_{T3} R G D c_{T3} A Y G C_{T3}	406 ± 63
C_{T3} R G D c_{T3} N W G C_{T3}	2084 ± 499
2nd generation	
C_{T3} R G D c_{T3} V Y G C_{T3}	211 ± 33
C_{T3} R G D c_{T3} A Y J C_{T3}	90 ± 15
C_{T3} R G D c_{T3} A W G C_{T3}	173 ± 35
C_{T3} R G D c_{T3} A Y a C_{T3}	156 ± 23
C_{T3} R G D c_{T3} A Y i C_{T3}	395 ± 153
C_{T3} R G D c_{T3} I Y G C_{T3}	386 ± 82
knottin-RGD	114 ± 8
cyclo-[KRGDf]	>10,000
cilengitide	>10,000
GRGDS	>10,000

J: D-Leu

Figure 2. IC_{50} values of 1st and 2nd generation bicyclic integrin $\alpha_5\beta_1$-binders.

C_{T3}GRGDXc_{T3}AYGC_{T3}, C_{T3}XRGDSc_{T3}AYGC_{T3}, Figure 1). We screened all 196 second generation bicycles at 5 μM and identified 18 bicycles (9%) with inhibition rates >70%. In a second screening of the best 20 hits at 2.5 μM 15 bicyclic peptides (75%) showed >70% inhibition and seven bicycles (35%) displayed >85% inhibition. Also, eight of the 20 bicycles exhibited higher inhibition values than C_{T3}RGDc_{T3}AYGC_{T3} itself (82% inhibition), for example, C_{T3}RGDc_{T3}VYGC_{T3} (90% inhibition) or C_{T3}RGDc_{T3}AYaC_{T3} (87% inhibition). Remarkably, the IC_{50} of the best inhibitor C_{T3}RGDc_{T3}AYJC_{T3} (90 nM, J: D-Leu, Figure 2) was even lower than that for knottin-RGD peptide (114 nM) and showed a 4-fold increased inhibition as compared to the first-generation binder C_{T3}RGDc_{T3}AYGC_{T3} (406 nM). The other five peptides all showed IC_{50} values below 400 nM, for example, C_{T3}RGDc_{T3}AYaC_{T3} (IC_{50} 156 nM). Hence, a change from "G" to "a" (i.e., D-Ala) at position 8, which is equivalent to the introduction of a single methyl group at the α-carbon, led to ~2.5-fold improved affinity for integrin $\alpha_5\beta_1$. For bicycles C_{T3}RGDc_{T3}AWGC_{T3} and C_{T3}RGDc_{T3}VYGC_{T3} comparable values were obtained (i.e. 173 and 211 nM, respectively), whereas the IC_{50}'s for bicycles C_{T3}RGDc_{T3}AYiC_{T3} (395 nM) and C_{T3}RGDc_{T3}IYGC_{T3} (386 nM) were almost identical to that of the lead.

Ala-Replacement Study for Selected $\alpha_5\beta_1$ Binders. To prove the unique binding affinity of the bicycles, we synthesized peptide libraries based on the sequences of the three highest-affinity $\alpha_5\beta_1$-binding bicycles, in which each amino acid was replaced by alanine, followed by CLIPS cyclization with **mT2** (see Figure S6A) to give the corresponding monocyclic peptides (for all Cys/Ala replacements), or with **T3** to give the corresponding bicyclic peptides (for all noncysteine replacements). Subsequently, we analyzed the libraries for the inhibition of $\alpha_5\beta_1$-binding in competition ELISA at 1 μM. The inhibitory values of the three best $\alpha_5\beta_1$-binding bicycles decreased massively when single amino acids in the loops were substituted by Ala (Figure 3). In general, Ala-replacements in the RGD loops gave the strongest effects. For example, replacing R or G in bicycle C_{T3}RGDc_{T3}AYJC_{T3} (Figure 3A), R or D in bicycle C_{T3}RGDc_{T3}AYaC_{T3} (Figure 3B), and R, G, or D in bicycle C_{T3}RGDc_{T3}AWGC_{T3} (Figure 3C) led to a complete loss of $\alpha_5\beta_1$-affinity (% inhibition at 1 μM $\leq$). Similarly, Ala-replacement of the cysteines (and hence loss of the bicyclic structure) also led to a massive decrease in binding strength. For example, substitution of either the N-terminal L-cysteine or the middle D-cysteine ("opening" of RGD-loop) led to a complete loss of $\alpha_5\beta_1$-affinity for bicycles C_{T3}RGDc_{T3}AYaC_{T3} and C_{T3}RGDc_{T3}AWGC_{T3} (% inhibition each <0). Also, when replacing the C-terminal L-cysteine, the inhibition values decreased significantly (e.g., to 26% for bicycle C_{T3}RGDc_{T3}AYJC_{T3} or to 45% for C_{T3}RGDc_{T3}AWGC_{T3}), albeit to a much lower extent than for the Ala-replacement of the amino acids in the RGD loop.

Finally, Ala-replacement of the non-RGD loop also resulted in significant losses of $\alpha_5\beta_1$-affinity, albeit to a somewhat lower extent. While the Y/A-replacement in C_{T3}RGDc_{T3}AYJC_{T3} showed a complete loss of inhibition (from 73% to <0%), Y/A-substitution in C_{T3}RGDc_{T3}AYaC_{T3} had a much reduced effect (inhibition from 60% to only 27%). In contrast to this, the J/A or G/A-replacement at the third position of the non-

A

Peptide	Inhibition at 1 μM [%]
C_{T3} R G D c_{T3} A Y J C_{T3}	73
A R G D c_{mT2} A Y J C_{mT2}	8
C_{T3} A G D c_{T3} A Y J C_{T3}	<0
C_{T3} R A D c_{T3} A Y J C_{T3}	<0
C_{T3} R G A c_{T3} A Y J C_{T3}	20
C_{mT2} R G D a A Y J C_{mT2}	<0
C_{T3} R G D c_{T3} A A J C_{T3}	33
C_{T3} R G D c_{T3} A Y A C_{T3}	<0
C_{mT2} R G D c_{mT2} A Y J A	26

J: D-Leu

B

Peptide	Inhibition at 1 μM [%]
C_{T3} R G D c_{T3} A Y a C_{T3}	60
A R G D c_{mT2} A Y a C_{mT2}	<0
C_{T3} A G D c_{T3} A Y a C_{T3}	<0
C_{T3} R A D c_{T3} A Y a C_{T3}	12
C_{T3} R G A c_{T3} A Y a C_{T3}	<0
C_{mT2} R G D a A Y a C_{mT2}	<0
C_{T3} R G D c_{T3} A A a C_{T3}	27
C_{T3} R G D c_{T3} A Y A C_{T3}	<0
C_{mT2} R G D c_{mT2} A Y a A	15

C

Peptide	Inhibition at 1 μM [%]
C_{T3} R G D c_{T3} A W G C_{T3}	82
A R G D c_{mT2} A W G C_{mT2}	<0
C_{T3} A G D c_{T3} A W G C_{T3}	<0
C_{T3} R A D c_{T3} A W G C_{T3}	<0
C_{T3} R G A c_{T3} A W G C_{T3}	1
C_{mT2} R G D a A W G C_{mT2}	<0
C_{T3} R G D c_{T3} A A G C_{T3}	27
C_{T3} R G D c_{T3} A W A C_{T3}	6
C_{mT2} R G D c_{mT2} A W G A	45

Figure 3. Ala-replacement study for $\alpha_5\beta_1$-binding bicycles (A) C_{T3}RGDc_{T3}AYJC_{T3}, (B) C_{T3}RGDc_{T3}AYaC_{T3}, and (C) C_{T3}RGDc_{T3}AWGC_{T3}. When cysteines were replaced by L- or D-Ala (A/a), peptides were cyclized using the bivalent scaffold **mT2**. For all other (noncysteine) replacements, peptides were cyclized using scaffold **T3**.

DOI: 10.1021/acscombsci.9b00081
ACS Comb. Sci. 2019, 21, 598−607

A

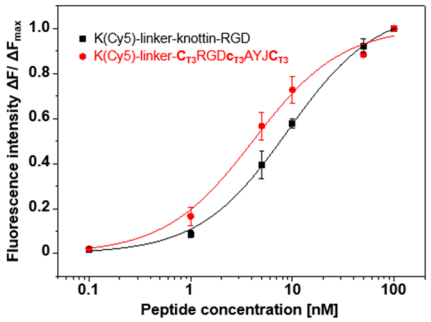

B

Peptide	K_d [nM] $\alpha_5\beta_1$	$\alpha_v\beta_3$
K(Cy5)-linker-C_{T3}RGDc_{T3}AYJC_{T3}	4.1	>100
K(Cy5)-linker-GRGDS*	>100	>100
cyclo-[K(K(Cy5)-linker)RGDf]*	>100	4.1
K(Cy5)-linker-knottin-RGD*	9.0	0.6

C

Peptide	IC_{50} [nM] $\alpha_5\beta_1$	$\alpha_v\beta_5$	$\alpha_v\beta_3$
C_{T3}RGDc_{T3}AYJC_{T3}	90 ± 15	>10,000	1,019 ± 137
C_{T3}RGDc_{T3}AYaC_{T3}	156 ± 23	> 4,000	992 ± 103
C_{T3}RGDc_{T3}AWGC_{T3}	173 ± 35	>10,000	1,885 ± 234
knottin-RGD*	114 ± 8	76 ± 7	38 ± 5
cyclo-[KRGDf]*	>10,000	182 ± 29	35 ± 6
cilengitide*	>10,000	26 ± 6	121 ± 18
GRGDS$	>10,000	~6,500	~5,000

J: D-Leucine

Figure 4. (A) Concentration-dependent, normalized fluorescence signals for K(Cy5)-linker-C_{T3}RGDc_{T3}AYJC_{T3} and K(Cy5)-linker-knottin-RGD binding to integrin $\alpha_5\beta_1$ (triplicate experiment). (B) Overview of equilibrium dissociation constants (K_d) as determined by SPFS. Values for $\alpha_5\beta_1$ were obtained by applying the 3D-hydrogel surface architecture. Values for $\alpha_v\beta_3$ were obtained by applying the thiol SAM surface architecture; (C) IC_{50} values for three structurally fully optimized bicycles, knottin-RGD and *cyclo*-[KRGDf]. Each concentration was tested in triplicate. IC_{50} values were calculated via nonlinear regression analysis. *,$These values were determined previously (* → ref 21, $ → ref 22).

RGD loop in bicycles C_{T3}RGDc_{T3}AYJC_{T3} and C_{T3}RGDc_{T3}AWGC_{T3} also led to a complete loss of integrin affinity. Much to our surprise, a simple change from D- to L-alanine at the third position of the non-RGD loop in bicycle C_{T3}RGDc_{T3}AYaC_{T3} also resulted in a total loss of $\alpha_5\beta_1$-binding activity, thus exemplifying the fact that very subtle structural changes in the bicycles can have a drastic effect on their binding activities.

Determination of Affinity Binding Constants (K_d). Determination of IC_{50} values provides an indirect method to estimate the corresponding binding affinities. In order to be able to directly observe the bicycle-integrin interactions, we employed an optical approach by combining surface plasmon resonance (SPR) with surface plasmon-enhanced fluorescence spectroscopy (SPFS). For this, we modified $\alpha_5\beta_1$-selective bicycle C_{T3}RGDc_{T3}AYJC_{T3}, linear GRGDS, *cyclo*-[KRGDf], and knottin-RGD with a linker (K-PPPSG(Abz)SG; Abz = 4-aminobenzoic acid; abbreviated hereafter as "K(Cy5)-linker") based on studies by Pallarola et al.[29] In the first SPR experiment, the binding of RGD-bicycle to integrins attached to the gold sensor surface was monitored directly from induced changes in the refractive index (data not shown). However, this approach did not provide sufficient sensitivity, probably because of the low molecular weight of the bicycles (~2 kDa). Therefore, we labeled the peptides with a fluorescent Cy5-tag and used its absorption band to locally excite the fluorescence signal close to the gold sensor surface carrying the immobilized integrins. This approach increases the fluorescence signal originating from peptide binding at the surface, which allowed us to measure the kinetics of the peptide-integrin interaction.[30] Dissociation equilibrium constants (K_d) of selected peptides were determined for both $\alpha_5\beta_1$ and $\alpha_v\beta_3$ integrins by real-time fluorescence signal analysis upon Cy5-labeled peptide binding to the integrin-anchored surface at various different concentrations using either a 2D-architecture with thiol SAM (data not shown),[21] or a 3D-hydrogel matrix of ~100 nm thick. The latter provided a significantly higher signal to noise ratio because it allowed to avoid the effect of quenching. Binding was measured at 0.1, 1.0, 10, and 100 nM, normalized to ΔF_{max} (value measured at saturation) and fitted via a Langmuir isotherm model (Figure 4A). For the interaction of bicycle K(Cy5)-linker-C_{T3}RGDc_{T3}AYJC_{T3} with integrin $\alpha_5\beta_1$, a K_d of 4.1 nM was determined (Figure 4B). Interestingly, this value indicates a substantially higher affinity as compared to knottin-RGD (K_d = 9 nM). It is worth noting that competition ELISA values revealed a much lower difference in IC_{50} for knottin-RGD and bicycle K(Cy5)-linker-C_{T3}RGDc_{T3}AYJC_{T3} (Figure 4B), which can be ascribed to the impact of attached Cy5-linker. For *cyclo*-[K(K(Cy5)-linker)RGDf] and K(Cy5)-linker-GRGDS binding in SPFS was not observed for integrin $\alpha_5\beta_1$, in accordance with the IC_{50} measurements. The additional SPFS results for the affinity interaction with integrin $\alpha_v\beta_3$ confirmed the high selectivity of bicycle K(Cy5)-linker-C_{T3}RGDc_{T3}AYJC_{T3} between both integrins $\alpha_v\beta_3$ and $\alpha_5\beta_1$ in accordance with ELISA IC_{50} measurements.

Selectivity Studies. Finally, we investigated the integrin selectivity of the three highest affinity $\alpha_5\beta_1$ integrin-binders via competition ELISA (Figure 4C). Bicycles C_{T3}RGDc_{T3}AYJC_{T3} and C_{T3}RGDc_{T3}AWGC_{T3} showed excellent selectivity over integrin $\alpha_v\beta_5$ (IC_{50} each >10 000 nM) with a selectivity ratio $\alpha_5\beta_1/\alpha_v\beta_5$ of <0.009 and <0.017, respectively (ratio of corresponding IC_{50} values). The selectivity over $\alpha_v\beta_3$ was also quite substantial, but not as good as for $\alpha_v\beta_5$ (IC_{50} = 1019 nM and 1185 nM, respectively), with a selectivity ratio $\alpha_5\beta_1/\alpha_v\beta_3$ of approximately 0.09. Bicycle C_{T3}RGDc_{T3}AYaC_{T3}, however, exhibited significantly lower selectivities (ratios of only 0.034 for $\alpha_5\beta_1/\alpha_v\beta_5$ and 0.157 for $\alpha_5\beta_1/\alpha_v\beta_3$). These data nicely illustrate the fact that the bicyclic RGD-peptide platform represents an excellent alternative to the high-affinity $\alpha_5\beta_1$ integrin-binder knottin-RGD, which shows basically no selectivity in integrin-binding.

Structural Assignment of Individual Amino Acids in C_{T3}RGDc_{T3}AYJC_{T3} via 2D NMR. Individual amino acids were identified through their H_α/C_α chemical shifts from the edited HSQC (Figure S-8), as well as the number and chemical shift of the side-chain resonances as revealed through 2D TOCSY (Figure S-9). The residue easiest to identify belonged to the phenol side chain of the tyrosine. The aromatic protons at 7.11 and 6.83 ppm were assigned ortho and meta to the phenol, respectively, and could be connected to the carbons at 133.3 and 118.3 ppm, respectively. Using a $^1H-^{13}C$ HMBC long-range coupling experiment, the H_α and H_β protons of the tyrosine residue were identified at 4.44 ppm and 3.03/2.90 ppm, while the corresponding C_α and C_β were identified at 58.9 and 38.2 ppm, respectively, via a 1-bond $^1H-^{13}C$ HSQC correlation experiment (Figure S-8). These shifts were consistent with a random coil conformation as opposed to a stable α helix or β sheet structure. An identical analysis was

DOI: 10.1021/acscombsci.9b00081
ACS Comb. Sci. 2019, 21, 598−607

performed for all readily identifiable amino acid residues, which yielded an overall random coil conformation for the RGD-bicyclic peptide (Figure 5A). Ideally, the bicyclic peptide

A

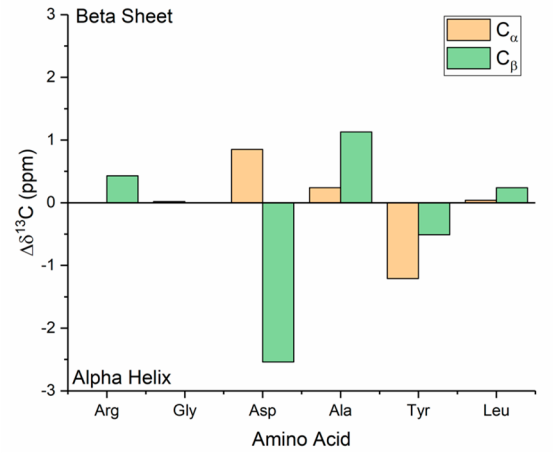

B

Residue	T_1 (s) Linear	T_1 (s) Bicycle	T_2 (s) Linear	T_2 (s) Bicycle
Gly	0.59	0.64	0.22	0.15
Ala	0.51	0.57	0.32	0.22
Asp	0.49	0.49	0.28	0.21
Tyr-δ	1.50	1.54	0.66	0.45
Tyr-ε	2.02	2.19	0.85	0.57

Figure 5. (A) Chemical shift difference plots for C_α and C_β calculated by $\Delta\delta^{13}C_\alpha = \Delta\delta^{13}C_{\alpha,rc} - \Delta\delta^{13}C_{\alpha,i}$ and $\Delta\delta^{13}C_\beta = \Delta\delta^{13}C_{\beta,i} - \Delta\delta^{13}C_{\beta,rc}$ (i = measured amino acid in bicycle, rc = random coil). Positive values reflect more β-sheet character while negative values represent more α-helical character. Amino acids that are close to the baseline are indicative of random coil structures, show both α-helical and β-sheet character, or alternatively structured sequences; (B) NMR relaxation times T_1 and T_2 as a function of amino acid residue.

should not have the tendency to either polymerize or aggregate in solution. To determine the effect of structuring the peptide by linking the peptide chain to a central mesityl moiety via the cysteine residues, T_1 and T_2 NMR relaxation measurements were undertaken for both the free chain peptide and bicyclic compound. T_1 relaxation for protons arises primarily through dipole−dipole interactions with neighboring nuclei that occur at the Larmour precession frequency, usually via molecular motion. T_2 relaxation involves the loss of spin coherence in the XY plane through variations in local magnetic fields of any frequency interacting with the nuclear spin. As both of these parameters involve molecular motion, they can be sensitive probes for phenomena, such as polymerization, aggregation, and complexation, which affect the rotational correlation time of the molecule. The residues that were most readily identifiable in both the free and bicyclic peptide were $H_{\alpha,Gly}$, $H_{\beta,Ala}$, $H_{\delta,Asp}$, $H_{\delta,Tyr}$, and $H_{\varepsilon,Tyr}$ (Figure 5B). In all cases, the T_1 values of these protons deviated less than 10% between the free and bicyclic forms, indicating that overall the molecular rotation of the molecule remains relatively unchanged. The T_2 values decreased slightly more, reflecting the increase in rigidity of the peptide, however not significantly enough to indicate dimerization or aggregation. Therefore, it can be concluded with relative certainty that these compounds exist as monomers in solution.

Membrane Binding on Integrin-Expressing Adipose-derived Stem Cells (ASC). To prove that RGD-bicycles also bind to integrins in their natural environment of the cell membrane, we labeled human adipose-derived stem cells (ASC, express integrin subunits α_5 and β_1) with the Cy5-functionalized, $\alpha_5\beta_1$-selective bicycle peptide K(Cy5)-linker-$\mathbf{C}_{T3}$RGD$\mathbf{c}_{T3}$AWG$\mathbf{C}_{T3}$ together with two scrambled variants of this bicycle (AWG → WGA and RGD → GDR, respectively) as well as the $\alpha_v\beta_3$-selective bicycle peptide $\mathbf{C}_{T3}$HPQ$\mathbf{c}_{T3}$RGD$\mathbf{c}_{T3}$,[21] and benchmark RGD-peptides knottin-RGD, *cyclo*-[KRGDf] and GRGDS, and detected fluorescence emission via confocal microscopy. The $\alpha_5\beta_1$-selective bicycle showed similar staining levels (Figure 6A) as compared to Cy5-labeled benchmark knottin-RGD (Figure 6E), while the $\alpha_v\beta_3$-selective bicycle $\mathbf{C}_{T3}$HPQ$\mathbf{c}_{T3}$RGD$\mathbf{c}_{T3}$ (Figure 6D) and benchmarks *cyclo*-[KRGDf] (Figure 6F) and GRGDS (Figure 6G) were virtually silent under these conditions. Control studies with scrambled RGD-bicycle $\mathbf{C}_{T3}$GDR$\mathbf{c}_{T3}$AWG$\mathbf{C}_{T3}$ (Figure 6B) showed hardly any traces of cell-staining, which proves the essential role of RGD for binding to membrane integrins. Moreover, the scrambled bicycle $\mathbf{C}_{T3}$RGD$\mathbf{c}_{T3}$WGA$\mathbf{C}_{T3}$ (Figure 6C) showed mediocre staining levels, albeit much weaker than observed for the parent bicycle, which proves the fact that binding is unequivocally AWG-sequence specific. The cell-staining data further illustrate the high potential of these highly integrin-selective RGD-bicycles as powerful markers of specific integrin-expression on live cells.

Screening for $\alpha_v\beta_5$-Binding Peptides. Finally, the fact that a selective integrin $\alpha_v\beta_5$-binder has not yet been reported in the literature encouraged us to extend the RGD-bicycle library screening to the search for $\alpha_v\beta_5$-binding bicycles. Integrin $\alpha_v\beta_5$ is an important mediator of cell adhesion and spreading,[31] among others, by internalizing conformationally modified vitronectin.[32] However, this integrin has been much less investigated as compared to integrins $\alpha_v\beta_3$ and $\alpha_5\beta_1$, and its action is generally described in alignment with $\alpha_v\beta_3$.[33−35] For example, both integrins $\alpha_v\beta_3$ and $\alpha_v\beta_5$ individually direct human cardiac myofibroblast differentiation via activation of TGF-β1.[36] Moreover, $\alpha_v\beta_5$ promoted angiogenesis induced by VEGF in corneal models in vivo, while $\alpha_v\beta_3$ supported bFGF-induced angiogenesis.[37]

Screening of our first-generation bicycle libraries for integrin $\alpha_v\beta_5$ revealed that only one out of 672 peptides showed more than 50% inhibition of knottin-RGD-$\alpha_v\beta_5$ binding ($\mathbf{C}_{T3}$RGD$\mathbf{c}_{T3}$NWG$\mathbf{C}_{T3}$). It is interesting to note, though, that exactly the same peptide was also identified as a first-generation binder to $\alpha_5\beta_1$ (vide supra). Approximately 94% of the RGD-bicycles showed <25% inhibition, revealing a clearly suboptimal positioning of the "RGD"-motif within the various bicycles tested. We determined a relatively high IC_{50} value of 1.46 μM for this lead (Figure 7), for which the $\alpha_v\beta_5$-inhibiting ability was much lower than that of knottin-RGD (76 nM), *cyclo*-[KRGDf] (182 nM), and cilengitide (26 nM). We then designed and synthesized second generation libraries (in total 196 peptides) based on the lead motif "NWG" and screened these for improved $\alpha_v\beta_5$-inhibiting activity at 5 μM concentration. Much to our surprise, not a single peptide exhibited an increased extent of $\alpha_v\beta_5$-inhibition in the

DOI: 10.1021/acscombsci.9b00081
ACS Comb. Sci. 2019, 21, 598−607

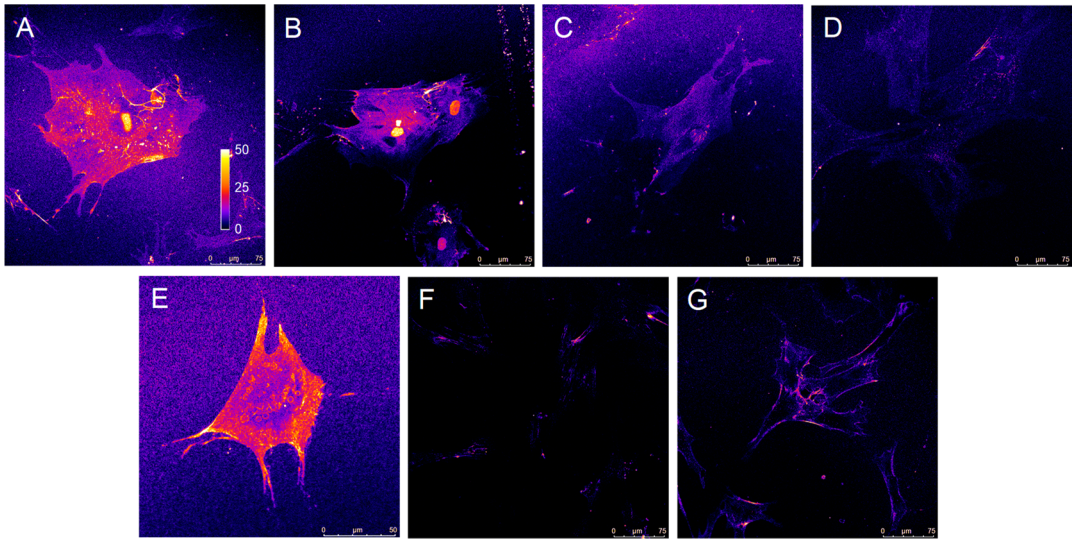

Figure 6. Confocal microscopy images of adipose-derived stem cells (ASC) incubated with (A) the $\alpha_5\beta_1$-selective bicycle Cy5-linker-$\mathbf{C}_{T3}$RGD$\mathbf{c}_{T3}$AWG$\mathbf{C}_{T3}$, (B) the structural variant with a scrambled AWG-loop (i.e., bicycle Cy5-linker-$\mathbf{C}_{T3}$RGD$\mathbf{c}_{T3}$WGA$\mathbf{C}_{T3}$), (C) the structural variant with a scrambled RGD-loop (i.e., bicycle Cy5-linker-$\mathbf{C}_{T3}$GDR$\mathbf{c}_{T3}$AWG$\mathbf{C}_{T3}$), (D) the $\alpha_v\beta_3$-selective bicycle Cy5-linker-$\mathbf{C}_{T3}$HPQ$\mathbf{c}_{T3}$RGD$\mathbf{c}_{T3}$, and benchmark peptides (E) Cy5-linker-knottin-RGD, (F) *cyclo*-[K(K(Cy5)-linker)RGDf], and (G) K(Cy5)-linker-GRGDS. Cells were incubated on glass coverslips for at least 4 days, followed by addition of Cy5-labeled peptides for 10 min at 4 °C, washing, fixation with 4% PFA, and finally confocal analysis. All images were acquired under identical imaging conditions and processed via ImageJ (LUT: Fire). The contrast is shown in arbitrary units (au): 0, no fluorescence; 50, maximum fluorescence. Images were taken at, or very close to, the basal membrane to ensure an optimal visualization of plasma membrane labeling. We want to explicitly emphasize that cytosolic labeling was thereby not observed for these cells.

Peptide	IC_{50} [nM]
1st generation	
$\mathbf{C}_{T3}$ R G D $\mathbf{c}_{T3}$ N W G $\mathbf{C}_{T3}$	1457 ± 452
2nd generation	
$\mathbf{C}_{T3}$ R G D $\mathbf{c}_{T3}$ N W f $\mathbf{C}_{T3}$	3668 ± 1407
$\mathbf{C}_{T3}$ R G D $\mathbf{c}_{T3}$ N W a $\mathbf{C}_{T3}$	650 ± 104
$\mathbf{C}_{T3}$ G R G D a $\mathbf{c}_{T3}$ N W G $\mathbf{C}_{T3}$	1150 ± 206
knottin-RGD	76 ± 7
cyclo-[KRGDf]	182 ± 29
cilengitide	26 ± 5
GRGDS	> 10,000

Figure 7. IC_{50} values of 1st and 2nd generation of RGD-bicyclic integrin $\alpha_v\beta_5$-binders.

screening as compared to the lead itself, while only four second generation bicycles showed more than 50% inhibition. Two of these, that is, bicycles $\mathbf{C}_{T3}$GRGDa$\mathbf{c}_{T3}$NWG$\mathbf{C}_{T3}$ and $\mathbf{C}_{T3}$RGD$\mathbf{c}_{T3}$NWa$\mathbf{C}_{T3}$, exhibited lower IC_{50} values (i.e., 1150 and 650 nM, respectively) compared to those of the lead (crude peptides used for initial screening, IC_{50} values determined using HPLC-purified bicycles), whereas $\mathbf{C}_{T3}$RGD$\mathbf{c}_{T3}$NWf$\mathbf{C}_{T3}$ had a much higher IC_{50} values (>3.5 μM, Figure 7). However, the binding affinities of these peptides were still much lower compared to that of the control RGD peptides, which reveals that the bicyclic RGD-peptide platform used seems not too well suited for identifying high-affinity $\alpha_v\beta_5$-binders.

CONCLUSION

The screening of partially randomized RGD-bicycle libraries was successfully applied in the search for integrin $\alpha_5\beta_1$-binders, eventually yielding three high-affinity second-generation bicyclic peptides, that is, $\mathbf{C}_{T3}$RGD$\mathbf{c}_{T3}$AYJ$\mathbf{C}_{T3}$ (J = D-Leu, IC_{50} = 90 nM), $\mathbf{C}_{T3}$RGD$\mathbf{c}_{T3}$AYa$\mathbf{C}_{T3}$ (IC_{50} = 156 nM), and $\mathbf{C}_{T3}$RGD$\mathbf{c}_{T3}$AWG$\mathbf{C}_{T3}$ (IC_{50} = 173 nM), with very good selectivities over integrin $\alpha_v\beta_5$ (selectivity ratios $\alpha_5\beta_1/\alpha_v\beta_5$ from <0.007 to <0.034) and moderate selectivities over $\alpha_v\beta_3$ (selectivity ratios $\alpha_5\beta_1/\alpha_v\beta_3$ of 0.09−0.157). Therefore, these bicycles represent an attractive structural platform to target $\alpha_5\beta_1$, be it in the context of therapeutic applications, biomaterial functionalization, or in vitro/in vivo tracers.

MATERIALS AND METHODS

Parts of the procedures have already been described in ref 21.

Reagents and Chemicals. Incubation and washing buffers were prepared using standard protocols. Recombinant human integrins were purchased from R&D Systems (Minneapolis, USA). Strep-HRP (streptavidin−horseradish peroxidase conjugate, Southern-Biotech, Birmingham, USA), was diluted 1:1000 for ELISA experiments. Amino acids were purchased from Iris Biotech (Marktredwitz, Germany) and Matrix Innovation (Quebec, Canada). Resins were purchased from Rapp Polymere (Tübingen, Germany) and Merck (Darmstadt, Germany). $MnCl_2{\cdot}4H_2O$, 1,3,5-tris(bromomethyl)benzene (**T3**), 1,2-bis(bromomethyl)benzene (**oT2**), 1,3-bis(bromomethyl)benzene (**mT2**), 2,6-bis(bromomethyl)-pyridine (**mP2**), 1,4-bis(bromomethyl)benzene (**pT2**), 2,2-dithiobis(5-nitropyridine) (DTNP), ethyl-(dimethylaminopropyl) carbodiimide (EDC), *N*-hydroxysuccinimide (NHS), ethanolamine, Tween 20, ethylene glycol, acetic acid, and sodium acetate for the preparation of acetate buffer were purchased from Sigma-Aldrich (Steinheim, Germany). $CaCl_2{\cdot}2H_2O$, $MgCl_2{\cdot}6H_2O$, and phosphate buffered saline (PBS) were purchased from Merck (Darmstadt, Germany). Tween 80 was purchased from Faryon (Capelle, The Netherlands) and I-Block was purchased from Tropix

DOI: 10.1021/acscombsci.9b00081
ACS Comb. Sci. 2019, 21, 598−607

(Bedford, USA). Disulfo-Cy5-NHS ester was purchased from Cyandye (Sunny Isles Beach, USA). Dithiolaromatic PEG6-carboxylate (thiol-COOH; SPT0014A6) and dithiolaromatic PEG3 (thiolPEG); SPT-0013) were purchased from Senso-Path Technologies (Bozeman, USA). Sodium para-tetrafluor-ophenol-sulfonate (TFPS) and *S*-3-(benzoylphenoxy)propyl ethethanethioate (thiol-benzophenone) were synthesized at the Max Planck Institute for Polymer Research (Mainz, Germany) according to literature.[38,39] A poly(*N*-isopropyla-crylamide)-based terpolymer with 94:5:1 molar ratio of *N*-isopropylacrylamide, methacrylic acid, and 4-methacryloyloxy benzophenone (pNIPAAm) were synthesized as previously described.[40,41]

Peptide Synthesis. *General Information.* Peptide syntheses were carried out on fully automated peptide synthesizers from MultiSyntech (Syro, 2 μmol scale for libraries) or Gyros Protein Technologies (Symphony) via Fmoc-based solid-phase peptide synthesis on Rink-amide resin using standard protocols. The couplings of L- and D-cysteines were performed manually using 2,4,6-trimethylpyridine as base to prevent racemization. Knottin-RGD peptide, *cyclo*-[KRGDf], and biotinylated knottin-RGD peptide were synthesized according to previous published protocols.[21,22] For IC_{50} determination and selectivity experiments, all peptides were purified by preparative HPLC on an RP-C18 column (Reprosil-Pur 120 C18-AQ 150 × 20 mm, Dr. Maisch GmbH, Ammerbuch, Germany) using an MeCN/H_2O gradient (5−65%) including 0.05% TFA, followed by lyophilization (Christ Alpha 2−4 LDplus). Library screening and inhibition experiments with single-loop peptides were carried out using nonpurified peptides. For all amino acids used, see Supporting Information.

Synthesis of Bicyclic Peptide Libraries. Linear peptide libraries (2 μmol) were dissolved in 0.5 mL of DMF. 1,3,5-Tris(bromomethyl) benzene (**T3**) in DMF (4.1 mM, 0.5 mL) and ammonium bicarbonate (150 mM, 0.5 mL) were added and the combined solutions mixed. After 1 hour at r.t., the reaction was quenched with 0.5% ethanethiol (in 1:1 DMF/H_2O, 0.1 mL). The bicyclic peptide libraries were freeze-dried using a Genevac HT-4X evaporation system. For a list of all applied amino acids, see Table S-1.

Synthesis of Bicyclic Peptides. To linear peptides dissolved at 0.5 mM in 1:3 MeCN/H_2O, 1.1 equiv of 1,3,5-tris(bromomethyl) benzene (**T3**) dissolved in MeCN, and 1.4 equiv ammonium carbicarbonate (0.2 M solution in H_2O) were added and shaken for 60 min. After completion (monitored by UPLC), the reaction was quenched with 10% TFA/H_2O to pH < 4, followed by lyophilization.

Peptide Labeling with Cy5. Peptides with an N-terminal amine were dissolved at 4 mM in DMSO, followed by adding disulfo-Cy5 NHS (1 equiv, 20 mg/mL in DMSO) and DIPEA (10 equiv). After completion (30−60 min), the reaction was quenched with 10% TFA/H_2O, using twice the volume of DIPEA, and subsequently purified via HPLC.

ELISA. For composition of all buffers and detailed concentrations, see Table S-2.

Integrin Coating and Blocking. Plates were coated with 100 μL of a 0.5 μg/mL integrin solution in coating buffer onto 96-well NUNC Polysorp (overnight, 4 °C) followed by blocking with 150 μL of 1% I-Block in blocking buffer (60 min, r.t.) and 3× washing with 400 μL of washing buffer.

Library Screening. Peptide libraries (2 μmol) were dissolved at 10 mM in DMSO and further diluted with incubation buffer. After incubation with a fixed concentration of biotinylated knottin-RGD peptide in incubation buffer (15 min, r.t.), mixed solutions were added to the integrin-coated plates (90 min, r.t.), followed by 3× washing with washing buffer. Then, the plates were incubated with 100 μL of 1:1000 Strep-HRP in Strep-HRP buffer (60 min, r.t.). After they were washed 4×, they were incubated with 150 μL of substrate buffer containing 0.91 mM ABTS (2,2′-azino-bis(3-ethyl-benzothiazoline-6-sulfonic acid) and 0.006% H_2O_2 in substrate buffer (0.2 M Na_2HPO_4 adjusted to pH 4 using 0.2 M citric acid). Absorbance was measured after 45 min using a Molecular Devices Spectramax M2 plate reader.

IC_{50} Determination. Peptides were mixed in eight different concentrations (each 3-fold dilutions) with a fixed concentration of biotinylated knottin-RGD (both in incubation buffer, 15 min, r.t.), followed by incubation of the plates with peptide/biotinylated knottin-RGDsolutions for 90 min at room temperature. Strep-HRP and ABTS incubation steps were performed like described for library screening. All concentrations were tested in triplicate. IC_{50} values were calculated via nonlinear regression analysis using GraphPad Prism software and represent the peptide concentration at which 50% inhibition of biotinylated knottin binding is observed.

Surface Plasmon Resonance-Enhanced Fluorescence (SPFS). For the description of the optical system and sensor chip preparation, the reader is referred to the Supporting Information.

Immobilization of Ligand. Immobilization of integrin $\alpha_5\beta_1$ was performed in situ by amine coupling according to standard protocols. The surface reactions were monitored by SPR (Figure S5A). First, acetate buffer (ACT, pH 4) was flowed over the gold surface until a stable baseline in SPR signal was established. Then, the sensor surface carrying carboxylic groups on mixed thiol self-assembled monolayer (SAM) was reacted with 75 mg/mL EDC and 21 mg/mL NHS dissolved in water for 15 min. For the 3D hydrogel interface carrying higher density of carboxylic moieties in its open polymer network structure, the activation was performed by TFPS dissolved in water (c = 21 mg/mL). Recombinant human integrins (c = 10 μg/mL), dissolved in acetate buffer (pH = 4), was flowed over the activated sensor surface for 90 min to bind the integrin molecules via their amine groups to activated carboxylic groups. Finally, remaining active ester groups were inactivated by flowing 1 M ethanolamine solution over the gold surface for 15 min.

Measurement of Equilibrium Dissociation Constant K_d. For measuring the binding affinity of Cy5-labeled peptides to immobilized integrin ligands, PBS with 1 mM $CaCl_2$, 0.5 mM $MnCl_2$, 1 mg/mL BSA, and 0.05% Tween20 was used as running buffer. Different concentrations of the peptide (0.1, 1, 5, 10, 50, 100, and 1000 nM) were sequentially flushed over the sensor surface. Each concentration was allowed to react with the integrin for 30 min, followed by rinsing the surface with running buffer solution for 10 min. The affinity binding of target analyte was monitored in real-time by measuring the fluorescence intensity $F(t)$ originating from the close proximity to the sensor surface that was probed by resonantly excited surface plasmons (Figure S-5B). The fluorescence signal F gradually increases upon the affinity binding of target analyte, and for each concentration, the equilibrium fluorescence signal ΔF was determined as a difference between fluorescence baseline after 10 min rinsing with running buffer. The titration curve was established based on these values and fitted with a

DOI: 10.1021/acscombsci.9b00081
ACS Comb. Sci. 2019, 21, 598−607

Langmuir isotherm model [function $\Delta F = \Delta F_{max} c/(K_d + c)$] to determine the equilibrium dissociation constant K_d.

NMR. All NMR spectra were collected on a Bruker Avance III 500 MHz spectrometer equipped with a Prodigy BB cryoprobe at 298 K. Samples were prepared by dissolving the compounds in D_2O and adding a small amount of DSS for internal referencing. ^1H spectra were acquired using 32 scans and a relaxation delay of 3 s. 2D COSYDQF spectra with presaturation were acquired with a 6000 Hz spectral width in both dimensions using 2048 × 512 points and processed using 2048 × 512 points, 4 scans per increment and a relaxation delay of 1.5 s. 2D gradient TOCSY spectra with presaturation were acquired with a 5000 Hz spectral width in both dimensions using 1024 × 512 points and processed using 1024 × 1024 points, 8 scans per increment, a relaxation delay of 2 s, and a TOCSY mix time of 100 ms. A TOCSY spinlock field of 8.3 kHz was applied. 2D gradient ROESY spectra were acquired with a 6000 Hz spectral width in both dimensions using 4096 × 512 points and processed using 4096 × 512 points, 24 scans per increment, a relaxation delay of 1.5 s and a ROESY mix time of 0.3 s. A ROESY spinlock field of 5 kHz was applied. Multiplicity-edited $^1H-^{13}C$ HSQC spectra were acquired using a 6010 Hz spectral width in F2 and 18868 Hz spectral width in F1 using 1024 × 512 points and processed to 1024 × 1024 points, 2 scans per increment, relaxation delay of 1.5 s and 1-bond J_{CH} = 145 Hz. $^1H-^{13}C$ HMBC spectra were acquired using a 5319.1 Hz spectral width in F2 and 22321.4 Hz spectral width in F1 using 2048 × 512 points and processed to 2048 × 2048 points, 4 scans per increment, relaxation delay of 1.5 s and a long-range J_{CH} = 8 Hz.

T_1 measurements were performed by properly calibrating the 90-degree pulse length and then performing estimates using the 1D inversion recovery sequence with excitation sculpting water suppression. After the longest T_1 was determined to be approximately 2 s, a pseudo-2D inversion recovery experiment was performed with 10 separate delays of 8 scans each with a total longitudinal relaxation time of 10.3 s. T_2 measurements were acquired by first performing estimates using the 1D PROJECT-CMPG[42] sequence with presaturation water suppression. After the longest T_2 was determined to be approximately 1 s, a pseudo-2D PROJECT-CPMG sequence experiment with presaturation was performed with 12 separate delays of 8 scans each, a cycle time of 4 ms with a total longitudinal relaxation time of 10.3 s.

Cell Integrin Staining and Confocal Microscopy. Human adipose-derived stem cells (ASC) were obtained from the University Medical Center Nijmegen and grown using standard procedures and conditions. For the experiment, the cells were allowed to adhere on clean glass coverslips for at least 4 d until reaching approximately 40−50% confluency. Then, the glass coverslips were washed two times with cold HCG buffer (carbonate-buffered saline, pH 7.2, containing 140 mM NaCl, 5 mM KCl, 23 mM $NaHCO_3$, 10 mM HEPES, 10 mM glucose, 1 mM $CaCl_2$, 0.5 mM $MgCl_2$, and 0.5 mM $MnCl_2$) to remove nonadhered cells, followed by adding cold HCG buffer, and cooling of the glass coverslips to 4 °C. Afterward, the Cy5-labeled peptides added and allowed to incubate at 1 μM for 10 min at 4 °C, followed by at least five washing steps with HCG buffer, fixation with 4% paraformaldehyde solution in PBS pH 7.4 (20 min) and another four washing steps with HCG buffer. Subsequently, the cells were analyzed via confocal microscopy using a Leica TCS SP8 confocal microscope equipped with a supercontinuum white light laser (NKT Photonics) and water immersion objectives (63× W PL APO CS2, NA 1.2/40× W PL APO CS2, NA 1.1). The excitation wavelength was set to 633 nm, while fluorescence was detected from 646 to 778 nm. All images were acquired at identical imaging conditions, and processed via ImageJ (LUT: Fire).

■ ASSOCIATED CONTENT

Supporting Information

The Supporting Information is available free of charge on the ACS Publications website at DOI: 10.1021/acscombsci.9b00081.

List of amino acids applied in this study, parameters varied in the competition ELISA setups, UPLC/ESI-MS spectra of purified bicycles $\mathbf{C_{T3}}$RGD$\mathbf{c_{T3}}$AYJ$\mathbf{C_{T3}}$, $\mathbf{C_{T3}}$RGD$\mathbf{c_{T3}}$AYa$\mathbf{C_{T3}}$, and $\mathbf{C_{T3}}$RGD$\mathbf{c_{T3}}$AWG$\mathbf{C_{T3}}$, description of optical instrument for SPR and SPFS measurements, optical instrument for SPFS and SPR measurements, description of sensor chip preparation and immobilization of ligand, example of an SPR sensorgram showing covalent immobilization of integrin $\alpha_5\beta_1$ into a 3D hydrogel binding matrix and fluorescence signal kinetics acquired upon titration of K(Cy5)-linker-$\mathbf{C_{T3}}$RGD$\mathbf{c_{T3}}$AYJ$\mathbf{C_{T3}}$, description of screening of single-loop CLIPS variants, overview of bi- and trivalent scaffolds for the synthesis of mono- and bicyclic peptides, $\alpha_5\beta_1$-inhibitory capacities of various monocyclic CLIPS-variants, ^1H, $^1H-^{13}C$ HSQCED, HMBC, and $^1H-^1H$ TOCSY spectra of $\mathbf{C_{T3}}$RGD$\mathbf{c_{T3}}$AYJ$\mathbf{C_{T3}}$, and absolute absorbances of library screening for 1st and 2nd generation of $\alpha_5\beta_1$-binders (PDF)

■ AUTHOR INFORMATION

Corresponding Author

*Tel.: +31-320-225300. Fax: +31-320-225301. E-mail: p.timmerman@pepscan.com.

ORCID

Jakub Dostalek: 0000-0002-0431-2170

Peter Timmerman: 0000-0001-6687-5297

Author Contributions

The manuscript was written through contributions of all authors. D.B. and P.T. conceived the concept and analyzed the data. D.B. performed peptide syntheses, competition and binding ELISA experiments, and in vitro integrin staining experiments. V.J., N.G.Q., and J.D. designed, performed, and analyzed the SPR/SPFS experiments. P.B.W. performed and analyzed the NMR experiments. D.B., K.J., and P.T. analyzed the confocal images. D.B., P.B.W., and P.T. wrote the manuscript. All authors have given approval to the final version of the manuscript.

Notes

The authors declare the following competing financial interest(s): Pepscan is the inventor of the CLIPS technology and holds a patent on the synthesis of bicyclic peptides using 2-CLIPS technology.

■ ACKNOWLEDGMENTS

This project has received funding from the European Union's Horizon 2020 research and innovation program under the Marie Sklodowska-Curie grant agreement no. 64268. Prof.

DOI: 10.1021/acscombsci.9b00081
ACS Comb. Sci. 2019, 21, 598−607

Egbert Oosterwijk is kindly acknowledged for providing the stem cells.

REFERENCES

(1) Barczyk, M.; Carracedo, S.; Gullberg, D. Integrins. *Cell Tissue Res.* **2010**, *339*, 269−280.
(2) Goodman, S. L.; Picard, M. Integrins as therapeutic targets. *Trends Pharmacol. Sci.* **2012**, *33*, 405−412.
(3) Schwartz, M. A.; Schaller, M. D.; Ginsberg, M. H. Integrins: Emerging Paradigms of Signal Transduction. *Annu. Rev. Cell Dev. Biol.* **1995**, *11*, 549−599.
(4) Avraamides, C. J.; Garmy-Susini, B.; Varner, J. A. Integrins in angiogenesis and lymphangiogenesis. *Nat. Rev. Cancer* **2008**, *8*, 604−617.
(5) Goessler, U. R.; Bugert, P.; Bieback, K.; Stern-Straeter, J.; Bran, G.; Hörmann, K.; Riedel, F. Integrin expression in stem cells from bone marrow and adipose tissue during chondrogenic differentiation. *Int. J. Mol. Med.* **2008**, *21*, 271−279.
(6) Mierke, C. T.; Frey, B.; Fellner, M.; Herrmann, M.; Fabry, M. Integrin $\alpha_5\beta_1$ facilitates cell invasion through enhanced contractile forces. *J. Cell Sci.* **2011**, *124*, 369−383.
(7) Schwartz, M. A.; Ginsberg, M. H. Networks and crosstalk: Integrin signalling spreads. *Nat. Cell Biol.* **2002**, *4*, E65−E68.
(8) Kim, S.; Harris, M.; Varner, J. A. Regulation of integrin $\alpha_v\beta_3$-mediated endothelial cell migration and angiogenesis by integrin $\alpha_5\beta_1$ and protein kinase A. *J. Biol. Chem.* **2000**, *275*, 33920−33928.
(9) Danen, E. H. J.; Sonneveld, P.; Brakebusch, C.; Fässler, R.; Sonnenberg, A. The fibronectin-binding integrins $\alpha_5\beta_1$ and $\alpha_v\beta_3$ differentially modulate RhoA-GTP loading, organization of cell matrix adhesions, and fibronectin fibrillogenesis. *J. Cell Biol.* **2002**, *159*, 1071−1086.
(10) Takada, Y.; Ye, X.; Simon, S. The Integrins. *Genome Biol.* **2007**, *8*, 215.
(11) Kimura, R. H.; Levin, A. M.; Cochran, F. V.; Cochran, J. R. Engineered cystine knot peptides that bind $\alpha_v\beta_3$, $\alpha_v\beta_5$, and $\alpha_5\beta_1$ integrins with low-nanomolar affinity. *Proteins: Struct., Funct., Genet.* **2009**, *77*, 359−369.
(12) Kimura, R. H.; Teed, R.; Hackel, B. J.; Pysz, M. A.; Chuang, C. Z.; Sathirachinda, A.; Willmann, J. K.; Gambhir, S. S. Pharmacokinetically Stabilized Cystine Knot Peptides that bind Alpha-v-Beta-6 Integrin with Single-Digit Nanomolar Affinities for Detection of Pancreatic Cancer. *Clin. Cancer Res.* **2012**, *18*, 839−849.
(13) Kim, J. W.; Cochran, F. V.; Cochran, J. R. A Chemically Cross-Linked Knottin Dimer Binds Integrins with Picomolar Affinity and Inhibits Tumor Cell Migration and Proliferation. *J. Am. Chem. Soc.* **2015**, *137*, 6−9.
(14) Gan, Z.-R.; Gould, R. J.; Jacobs, J. W.; Friedman, P. A.; Polokoff, M. A. Echistatin. A Potent Platelet Aggregation Inhibitor from the Venom of the Viper, *Echis carinatus*. *J. Biol. Chem.* **1988**, *263*, 19827−19832.
(15) Kapp, T. G.; Rechenmacher, F.; Neubauer, S.; Maltsev, O. V.; Cavalcanti-Adam, E. A.; Zarka, R.; Reuning, U.; Notni, J.; Wester, H.-J.; Mas-Moruno, C.; Spatz, J. P.; Geiger, B.; Kessler, H. A Comprehensive Evaluation of the Activity and Selectivity Profile of Ligands for RGD-binding Integrins. *Sci. Rep.* **2017**, *7*, 39805.
(16) Stoeltzing, O.; Liu, W.; Reinmuth, N.; Fan, F.; Parry, G. C.; Parikh, A. A.; McCarty, M. F.; Bucana, C. D.; Mazar, A. P.; Ellis, L. M. Inhibition of integrin $\alpha_5\beta_1$ function with a small peptide (ATN-161) plus continuous 5-FU infusion reduces colorectal liver metastases and improves survival in mice. *Int. J. Cancer* **2003**, *104*, 496−503.
(17) Khalili, P.; Arakelian, A.; Chen, G.; Plunkett, M. L.; Beck, I.; Parry, G. C.; Shaw, D. E.; Mazar, A. P.; Rabbani, S. A. A non-RGD-based integrin binding peptide (ATN-161) blocks breast cancer growth and metastasis in vivo. *Mol. Cancer Ther.* **2006**, *5*, 2271−2281.
(18) Heckmann, D.; Meyer, A.; Laufer, B.; Zahn, G.; Stragies, R.; Kessler, H. Rational Design of Highly Active and Selective Ligands for the $\alpha_5\beta_1$ Integrin Receptor. *ChemBioChem* **2008**, *9*, 1397−1407.
(19) Rechenmacher, F.; Neubauer, S.; Polleux, J.; Mas-Moruno, C.; De Simone, M.; Cavalcanti-Adam, E. A.; Spatz, J. P.; Fässler, R.; Kessler, H. Functionalizing $\alpha_v\beta_3$- or $\alpha_5\beta_1$-selective integrin antagonists for surface coating: A method to discriminate integrin subtypes in vitro. *Angew. Chem., Int. Ed.* **2013**, *52*, 1572−1575.
(20) Kapp, T. G.; Di Leva, F. S.; Notni, J.; et al. *N*-Methylation of iso DGR Peptides: Discovery of a Selective $\alpha_5\beta_1$-Integrin Ligand as a Potent Tumor Imaging Agent. *J. Med. Chem.* **2018**, *61*, 2490−2499.
(21) Bernhagen, D.; Jungbluth, V.; Quilis, N. G.; Dostalek, J.; White, P. B.; Jalink, K.; Timmerman, P. Bicyclic RGD Peptides with Exquisite Selectivity for the Integrin $\alpha_v\beta_3$ Receptor Using a "Random Design" Approach. *ACS Comb. Sci.* **2019**, *21*, 198−206.
(22) Bernhagen, D.; De Laporte, L.; Timmerman, P. High-Affinity RGD-Knottin Peptide as a New Tool for Rapid Evaluation of the Binding Strength of Unlabeled RGD-Peptides to $\alpha_v\beta_3$, $\alpha_v\beta_5$, and $\alpha_5\beta_1$ Integrin Receptors. *Anal. Chem.* **2017**, *89*, 5991−5997.
(23) Timmerman, P.; Beld, J.; Puijk, W. C.; Meloen, R. H. Rapid and quantitative cyclization of multiple peptide loops onto synthetic scaffolds for structural mimicry of protein surfaces. *ChemBioChem* **2005**, *6*, 821−824.
(24) Li, P.; Roller, P. P. Cyclization strategies in peptide derived drug design. *Curr. Top. Med. Chem.* **2002**, *2*, 325−341.
(25) Baeriswyl, V.; Heinis, C. Polycyclic Peptide Therapeutics. *ChemMedChem* **2013**, *8*, 377−384.
(26) Timmerman, P.; Barderas, R.; Desmet, J.; Shochat, S.; Monasterio, A.; Casal, J. I.; Meloen, R. H.; et al. A combinatorial approach for the design of complementarity-determining region-derived peptidomimetics with in vitro anti-tumoral activity. *J. Biol. Chem.* **2009**, *284*, 34126−34134.
(27) Heinis, C.; Rutherford, T.; Freund, S.; Winter, G. Phage-encoded combinatorial chemical libraries based on bicyclic peptides. *Nat. Chem. Biol.* **2009**, *5*, 502−507.
(28) Dechantsreiter, M. A.; Planker, E.; Matha, B.; Lohof, E.; Jonczyk, A.; Goodman, S. L.; Kessler, H.; et al. *N*-Methylated Cyclic RGD Peptides as Highly Active and selective $\alpha_V\beta_3$ integrin antagonists. *J. Med. Chem.* **1999**, *42*, 3033−3040.
(29) Pallarola, D.; Bochen, A.; Boehm, H.; Rechenmacher, F.; Sobahi, T. R.; Spatz, J. P.; Kessler, H. Interface immobilization chemistry of cRGD-based peptides regulates integrin mediated cell adhesion. *Adv. Funct. Mater.* **2014**, *24*, 943−956.
(30) Bauch, M.; Toma, K.; Toma, M.; Zhang, Q.; Dostalek, J. Surface plasmon-enhanced fluorescence biosensors: a review. *Plasmonics* **2014**, *9*, 781−799.
(31) Asano, Y.; Ihn, H.; Yamane, K.; Kubo, M.; Tamaki, K. Increased Expression Levels of Integrin $\alpha_v\beta_5$ on Scleroderma Fibroblasts. *Am. J. Pathol.* **2004**, *164*, 1275−1292.
(32) Panetti, T. S.; McKeown-Longo, P. J. The $\alpha_v\beta_5$ integrin receptor regulates receptor-mediated endocytosis of vitronectin. *J. Biol. Chem.* **1993**, *268*, 11492−11495.
(33) Friedlander, M.; Theesfeld, C. L.; Sugita, M.; Fruttiger, M.; Thomas, M. A.; Chang, S.; Cheresh, D. A. Involvement of integrins $\alpha_v\beta_3$ and $\alpha_v\beta_5$ in ocular neovascular diseases. *Proc. Natl. Acad. Sci. U. S. A.* **1996**, *93*, 9764−9769.
(34) Hynes, R. O. A re-evaluation of integrins as regulators of angiogenesis. *Nat. Med.* **2002**, *8*, 918−921.
(35) Conroy, K. P.; Kitto, L. J.; Henderson, N. C. $\alpha\beta$ Integrins: Key Regulators of Tissue Fibrosis. *Cell Tissue Res.* **2016**, *365*, 511−519.
(36) Sarrazy, V.; Koehler, A.; Chow, M. L.; Zimina, E.; Li, C. X.; Kato, H.; Caldarone, C. A.; Hinz, B. Integrins $\alpha v\beta_5$ and $\alpha_v\beta_3$ promote latent TGF-β1 activation by human cardiac fibroblast contraction. *Cardiovasc. Res.* **2014**, *102*, 407−417.
(37) Friedlander, M.; Brooks, P. C.; Shaffer, R. W.; Kincaid, C. M.; Varner, J. A.; Cheresh, D. A. Definition of Two Angiogenic Pathways by Distinct α_v Integrins. *Science* **1995**, *270*, 1500−1502.
(38) Beines, P. W.; Klosterkamp, I.; Menges, B.; Jonas, U.; Knoll, W. Responsive Thin Hydrogel Layers from Photo-Cross-Linkable Poly(*N*-isopropylacrylamide) Terpolymers. *Langmuir* **2007**, *23*, 2231−2238.
(39) Gee, K. R.; Archer, E. A.; Kang, H. C. 4-Sulfotetrafluorophenyl (STP) esters: New water-soluble amine-reactive reagents for labeling biomolecules. *Tetrahedron Lett.* **1999**, *40*, 1471−1474.

DOI: 10.1021/acscombsci.9b00081
ACS Comb. Sci. 2019, 21, 598−607

(40) Junk, M. J. N.; Jonas, U.; Hinderberger, D. EPR spectroscopy reveals nanoinhomogeneities in the structure and reactivity of thermoresponsive hydrogels. *Small* **2008**, *4*, 1485−1493.
(41) Anac, I.; Aulasevich, A.; Junk, M. J. N.; Jakubowicz, P.; Roskamp, R. F.; Menges, B.; Jonas, U.; Knoll, W. Optical Characterization of Co-Nonsolvency Effects in Thin Responsive PNIPAAm-Based Gel Layers Exposed to Ethanol/Water Mixtures. *Macromol. Chem. Phys.* **2010**, *211*, 1018−1025.
(42) Aguilar, J. A.; Nilsson, M.; Bodenhausen, G.; Morris, G. A. Spin echo NMR spectra without J modulation. *Chem. Commun.* **2012**, *48*, 811−813.

DOI: 10.1021/acscombsci.9b00081
ACS Comb. Sci. 2019, 21, 598−607